Three-Dimensional Shear Wave Elastography Using Acoustic Radiation Force and a 2-D Row-Column Addressing (RCA) Array

Zhijie Dong, *Member, IEEE*, U-Wai Lok, Matthew R. Lowerison, Chengwu Huang, *Member, IEEE*, Shigao Chen, *Senior Member, IEEE*, and Pengfei Song, *Senior Member, IEEE*

***Abstract*—Acoustic radiation force (ARF)-based shear wave elastography (SWE) is a clinically available ultrasound imaging mode that noninvasively and quantitatively measures tissue stiffness. Current implementations of ARF-SWE are largely limited to 2-D imaging, which does not provide a robust estimation of heterogeneous tissue mechanical properties. Existing 3-D ARF-SWE solutions that are clinically available are based on wobbler probes, which cannot provide true 3-D shear wave motion detection. Although 3-D ARF-SWE based on 2-D matrix arrays have been previously demonstrated, they do not provide a practical solution because of the need for a high channel-count ultrasound system (e.g., 1024-channel) to provide adequate volume rates and the delicate circuitries (e.g., multiplexers) that are vulnerable to the long-duration "push" pulses. To address these issues, here we propose a new 3-D ARF-SWE method based on the 2-D row-column addressing (RCA) array which has a much lower element count (e.g., 256), provides an ultrafast imaging volume rate (e.g., 2000 Hz), and can withstand the push pulses. In this study, we combined the comb-push shear elastography (CUSE) technique with 2-D RCA for enhanced SWE imaging field-of-view (FOV). In vitro phantom studies demonstrated that the proposed method had robust 3-D SWE performance in both homogenous and inclusion phantoms. An in vivo study on a breast cancer patient showed that the proposed method could reconstruct 3-D elasticity maps of the breast lesion, which was validated using a commercial ultrasound scanner. These results demonstrate strong potential for the proposed method to provide a viable and practical solution for clinical 3-D ARF-SWE.**

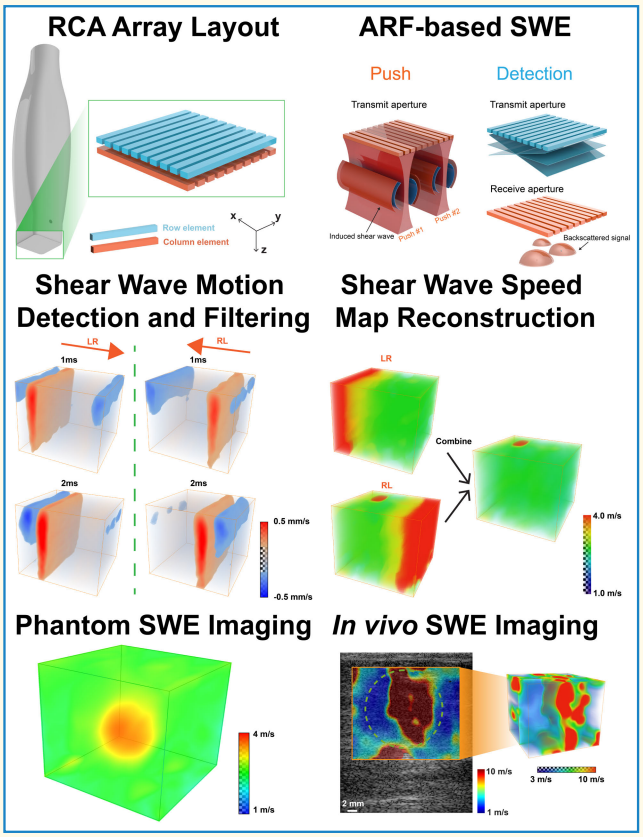

***Index Terms*—3-D shear wave elastography (SWE), acoustic radiation force (ARF), comb-push shear elastography (CUSE), row-column addressing (RCA) array, ultrafast ultrasound imaging.**

I. Introduction

ULTRASOUND elastography is a clinically available ultrasound imaging modality for assessing tissue stiffness, which is an essential biomarker for many clinical applications such as identifying malignant thyroid nodules [1], [2], assessing liver fibrosis [3], [4], and characterizing breast cancer [5]. There are two major groups of ultrasound elastography techniques: the first group is called strain elastography, which measures the tissue deformation induced by various forms of stress including probe compression [6], physiological motion [7], and acoustic radiation force (ARF) [8]. However, because of the practical challenges associated with assessing the applied stress, strain elastography only provides relative tissue stiffness measurement (e.g., a stiff lesion embedded in a soft background) [9]. The second group of methods is called shear wave elastography (SWE), which provides a direct assessment of tissue stiffness [9], [10], [11] by utilizing externally induced shear waves whose

Manuscript received 27 January 2024; accepted 10 February 2024. Date of publication 16 February 2024; date of current version 28 March 2024. This work was supported by the Department of Defense (DoD) through the Breast Cancer Research Program (BCRP) under Award W81XWH-21-1-0062 and Award W81XWH-21-1-0063. *(Corresponding author: Pengfei Song.)*

This work involved human subjects or animals in its research. Approval of all ethical and experimental procedures and protocols was granted by the Mayo Clinic Institutional Review Board (IRB).

Please see the Acknowledgment section of this article for the author affiliations.

Digital Object Identifier 10.1109/TUFFC.2024.3366540

Highlights

- **An ARF-based 3-D SWE method was proposed based on a 2-D RCA array with the comb-push technique integrated for enhanced SWE performance.**
- **The 3-D ARF-SWE method provides robust 3-D elasticity map reconstruction with a high 3-D imaging volume rate and short data acquisition.**
- **The proposed method presents a practical and cost-effective 3-D SWE solution for clinical implementations of 3-D tissue elasticity imaging.**

propagation speed is associated with tissue shear and Young's modulus. In practice, SWE uses shear waves induced by external vibration [12], [13], ARF [14], [15], or physical motion [16], [17].

Similar to the mainstream ultrasound imaging techniques, current SWE methods are primarily confined to 2-D imaging, which does not provide a comprehensive analysis of the shear wave signal that propagates in all 3-D. As a result, the reliability of the quantitative elasticity measurements may be compromised because of missing the shear wave signals that are not captured in the 2-D field-of-view (FOV) (e.g., out-of-plane shear wave signals). Although for homogeneous tissues, the lack of 3-D shear wave tracking may not result in unreliable SWE performance, for anisotropic tissue or a complex shear wave field (e.g., external vibration), 3-D shear wave detection becomes indispensable [18], [19], [20], [21], [22].

Conventional 3-D SWE techniques are mainly based on mechanically tilting, rotating, or translating of 1-D array transducers (e.g., wobbler) to stack 2-D SWE slices into 3-D volumes [23], [24]. However, these SWE techniques may not be considered true 3-D because they do not detect shear wave propagation in all 3-D. As such, these techniques do not provide unbiased 3-D shear wave speed estimation that gives rise to 3-D quantifications of shear elasticity. In addition, wobbler based 3-D SWE takes several seconds to scan the 3-D volume, making it susceptible to handheld probe movement and tissue motion.

Over the past decade, 2-D matrix arrays-based 3-D SWE methods enabled high volume rate acquisition as well as 3-D motion detection [16], [18], [25], [26]. Because the whole volume can be rapidly scanned with electronic steering, 2-D matrix arrays are capable of detecting 3-D shear wave motion for 3-D shear elasticity estimation. However, one limitation of 2-D matrix arrays is that a high channel-count ultrasound system (e.g., 1024-channel for a 32×32 element 2-D array) is required to provide an adequate volume rate for 3-D shear wave tracking. This requirement imposes a practical barrier to the widespread adoption of the technology because high channel-count ultrasound systems are very expensive and not commonly available. A common solution for this issue is to use multiplexing [27], [28] and micro-beamforming [29], [30], which effectively reduces the requirement of a high channel-count ultrasound system. However, multiplexing reduces the imaging volume rate, which makes it challenging to track 3-D shear wave motion [26]. In addition, the complex circuitry associated with multiplexing and micro-beamformers is vulnerable to the long-duration push pulses used in ARF-SWE.

Recently, 2-D row-column addressing (RCA) arrays have emerged as an enticing solution for addressing the issues of low volume rate and high channel count with 2-D matrix arrays. Two-dimensional RCA arrays do not use fully populated 2-D matrices for element distribution—instead, it uses bar-shaped elements arranged orthogonally as row elements and column elements [31], as shown in Fig. 1(a). As a result, the number of elements is reduced from $N \times N$ to $N+N$ (e.g., 16 384 to 256 elements), making them compatible with mainstream ultrasound systems. This design makes RCA arrays advantageous for 3-D SWE for several reasons: First, the significantly reduced element count eliminates the need for multiplexing and micro-beamforming, which makes 2-D RCA arrays suitable for generating ARF-based shear waves with long-duration push pulses. Second, when combined with a system that is equipped with software beamformers and massive parallel receive capability (e.g., capable of plane wave imaging), 2-D RCA arrays provide an ultrafast 3-D imaging volume rate (e.g., several thousand Hertz) that is ideal for 3-D shear wave tracking. In a previous study [32], we validated RCA-based 3-D shear wave detection by using both mechanical vibrations and ARF (by using a separate probe). In another study, Bernal et al. [33] used RCA arrays to detect passive shear waves. To date, a 3-D ARF-SWE approach based on the same 2-D RCA arrays (i.e., for both shear wave generation and detection) has not been reported, which is what we will present in this study.

The rest of this article is structured as follows. We first describe the workflow and sequences of the proposed method, followed by phantom studies and an in vivo case study on a breast cancer patient. The corresponding results will be presented in Section III. We finalize this article with discussions and conclusions.

II. Materials and Methods

A. Implementation and Optimization of 3-D ARF-SWE Based on the 2-D RCA Array

A custom-built RCA array (Daxsonics Ultrasound Inc., Halifax, NS, Canada; central frequency at 7 MHz with 65% bandwidth) and a Verasonics Vantage 256 system (Verasonics Inc., Kirkland, WA, USA) were used in this study for ARF-based shear wave generation and 3-D shear wave detection. The RCA array includes 128 row elements stacked on top of 128 column elements [Fig. 1(a)]. Thanks to the

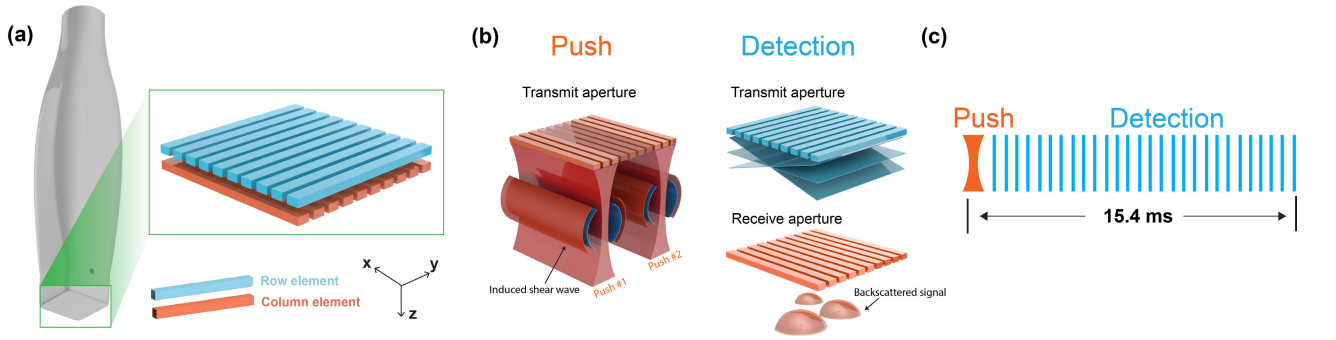

Fig. 1. (a) RCA array with orthogonally arranged row elements (distributed along the x-direction) and column elements (distributed along the y-direction). (b) Illustration of the push and detection schemes of the 3-D ARF-based SWE combined with CUSE. The column elements transmit two focused push beams to generate shear wave motion, followed by shear wave detection using the row elements for transmit focusing and column elements for receive focusing. (c) Timeline of the SWE sequence. The two push beams (400 μs each) were simultaneously (focused comb-push) or successively (marching comb-push) transmitted at first, followed by an ultrafast acquisition with 30 volumes at a 2000 Hz volume rate. The total duration of push-detection data acquisition was 15.4 ms.

TABLE I
THREE-DIMENSIONAL ARF-SWE IMAGING CONFIGURATIONS

Parameter	Value
Central frequency [MHz]	7
Bandwidth [%]	65
Sampling frequency [MHz]	27.78
Number of elements	256
Element spacing [um]	214
Push pulse frequency [MHz]	5
Push pulse length [us]	400
Push beam F-number for phantom study	2.92
Push beam F-number for *in vivo* study	1.46
Push beam focal depth range [mm]	10 – 25
Push beam voltage [V]	50
Detection pulse repetition interval (PRI) [ms]	65
Detection pulse repetition frequency (PRF) [Hz]	15385
Detection volume rate [Hz]	2000
Number of acquired volumes	30
Imaging depth [mm]	40
X-range [mm]	27.4
Y-range [mm]	27.4

simple design, the 2-D RCA array can sustain the long push pulses for ARF generation (e.g., hundreds of microseconds). The configurations of the RCA array as well as the 3-D SWE imaging sequences are reported in Table I.

In this study, we combined 2-D RCA with the comb-push shear elastography (CUSE) technique to achieve a large 3-D imaging FOV without the need for multiple push-detection data acquisitions [34]. As shown in Fig. 1(b), two focused push beams positioned at the edges of the transducer were simultaneously (focused comb-push) or successively (marching comb-push) [35] transmitted for shear wave generation using column elements (distributed along the y-direction). Because of the bar-shaped element, 2-D RCA arrays can only perform transmit focusing in 1-D, which results in plate-shaped shear waves that are focused in 1-D and planar in the orthogonal dimension [Fig. 1(b)]. Various push beam configurations were tested, and a final configuration of a push pulse with 400 μs duration and 5 MHz center frequency was used throughout the rest of the study, as detailed in Table I.

For 3-D shear wave detection, a compounding plane wave imaging sequence with seven compounding angles was used immediately after the push beam transmission, as shown in Fig. 1(b) and (c). The angular step size of 0.5° was used to mitigate grating lobes [36]. For detection, all row elements (distributed along the x-direction) were used to transmit, and all column elements were used to receive. As a result, the transmit focusing was along the x-direction, and the dynamic receive focusing was along the y-direction, which was aligned with the main propagation direction (y-direction) of the induced shear waves. A total of 30 volumes were acquired at a 2000 Hz volume rate. The final 3-D SWE sequence (including a single push and detection cycle) for the entire 3-D volume data acquisition only lasted 15.4 ms, which is significantly faster than existing 3-D SWE methods (e.g., a few seconds for wobbler based 3-D SWE [23], and around 128 ms for matrix array-based 3-D SWE with five push cycles and 1488 Hz volume rate [25]). Throughout the studies, a B-mode imaging sequence (50 Hz volume rate, 31 compounding angles) with real-time bi-planar visualization of 3-D volumes was used to provide scanning guidance and localize the targeted tissue, followed by the 3-D ARF-SWE acquisition.

For 3-D shear wave speed (SWS) map reconstruction, the following processes were implemented, as outlined in Fig. 2. First, 3-D in-phase quadrature (IQ) data were beamformed using delay-and-sum (DAS) beamforming [Fig. 2(a)], followed by shear wave motion estimation [Fig. 2(b)] using 1-D autocorrelation (window length = 4.5 wavelengths along z-direction) [37], [38]. Subsequently, bandpass filtering and

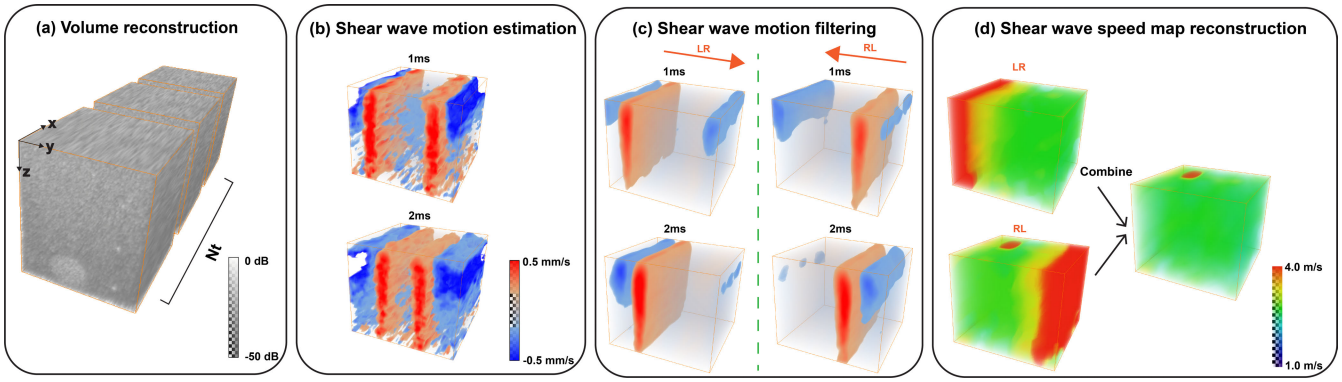

Fig. 2. Proposed 3-D SWE data processing steps. (a) IQ volumes acquired using the RCA array at an ultrafast volume rate (e.g., 2000 Hz) were beamformed. (b) Raw shear wave motions were calculated from acquired IQ volumes. (c) Filtered shear wave motions from left to right (LR) and from right to left (RL) were extracted using directional filtering and bandpass filtering. (d) Three-dimensional SWS maps from separated shear wave fields were reconstructed and combined to reconstruct the final 3-D SWS map.

directional filtering were applied to denoise and separate the shear wave particle velocity data into two directions (positive y-direction and negative y-direction), as shown in Fig. 2(c). Finally, the 3-D cross correlation [25], [39] method was used to reconstruct two 3-D SWS maps for each shear wave propagation direction with a step size of 12 wavelengths and an averaging window of 24 wavelengths along three directions, which were then combined into a final 3-D SWS map using the Tukey window [40], as shown in Fig. 2(d).

B. Acoustic Field Scan and Acoustic Output Measurements

The acoustic field and output for the push beams used in this study were assessed using both simulation and water tank measurements with hydrophones. The simulation was conducted using the Verasonics simulator. For the hydrophone measurement, a capsule hydrophone (HGL-0200, Onda Corporation, Sunnyvale, CA, USA), submerged in a water tank filled with deionized and degassed water using a water conditioner (AQUAS-10, Onda Corporation, Sunnyvale, CA, USA), was used to measure the 3-D acoustic pressure field of the push beams. The hydrophone was mounted on linear and rotary positioners (AIMS III, Onda Corporation, Sunnyvale, CA, USA) to scan the 3-D acoustic field, with 1-, 1-, and 2-mm step size in the x (lateral), y (elevational), and z (axial) dimensions, respectively. The Vantage system was synchronized with the capsule hydrophone and the scanning stage, and the water temperature was measured to calibrate the speed of sound. MI (derated at a rate of 0.3 dB/cm/MHz) and $I_{\mathrm{SPTA},0.3}$ were measured for the push beams with different focal depths (10–25 mm) and F-numbers (1.46 and 2.92).

C. Elasticity Phantom Studies

The performance of the proposed 3-D ARF-SWE method was first evaluated in a multipurpose multitissue ultrasound phantom (Model 040GSE, CIRS Inc., Norfolk, VA, USA) and an elasticity phantom (Model 049, CIRS Inc., Norfolk, VA, USA). For the multipurpose phantom, a homogenous region (shear wave speed of 2.60 $\pm$ 0.15 m/s [40]) was imaged to evaluate the accuracy of the shear wave speed measurement. For the elasticity phantom, four spherical lesion objects with different elasticity (SWS from 1.38 to 4.65 m/s) were imaged to test the 3-D SWE performance in heterogeneous tissue. The targeted lesions were located at a 10–20 mm depth with an approximate diameter of 10 mm, and a focal depth of 20 mm was used for the push beam with an F-number of 2.92. Both phantoms have an ultrasound attenuation of 0.5 dB/cm/MHz [41] and a speed of sound of 1540 m/s.

D. In Vivo Case Study

To further evaluate the in vivo performance of the proposed 3-D ARF-SWE method, a case study on a breast cancer patient was performed. The same subject was also imaged by a conventional clinical ultrasound system (General Electric Healthcare, Wauwatosa, WI, USA) with 2-D SWE [34], which was used as a reference for the newly developed 3-D ARF-SWE method. The in vivo protocols were approved by the Mayo Clinic Institutional Review Board (IRB), and written informed consent was obtained before scanning. To improve the signal-to-noise ratio (SNR) of the shear wave signals, the F-number of the push beams was reduced to 1.46, and a marching comb-push with successive transmission of focused push beams was used. The total data acquisition time for the 3-D SWE sequence was approximately 16 ms.

III. Results

A. Acoustic Field Scan and Acoustic Output Measurements

Fig. 3 shows the simulated and measured 3-D acoustic fields of the comb-push beams, as well as two representative slices along the y-z and x-y dimensions. The measured fields were closely matched with the simulation results. Due to the element sensitivity difference resulting from probe manufacturing, the acoustic fields of the left push beam and right push beam were not identical.

The MI values measured from 5 to 30 mm for push beams with two different F-numbers (i.e., 2.92 and 1.46) and different focal depths were plotted in Fig. 4. A maximum MI value of 1.23 was measured when the push beam was focused

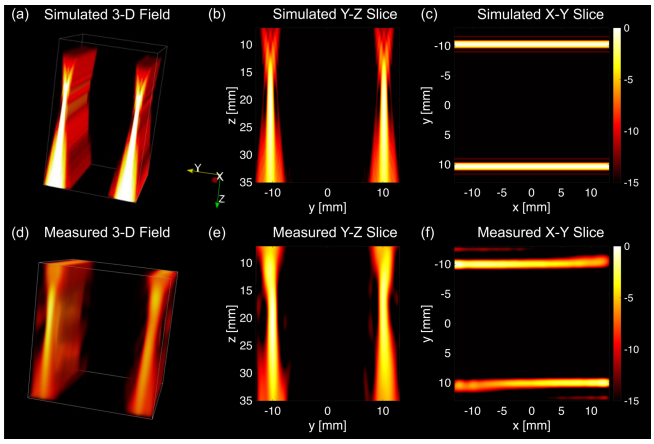

Fig. 3. Simulated and measured 3-D acoustic fields of the comb-push beams generated by the RCA array. (a) Simulated 3-D acoustic field of the comb-push beams. (b) Simulated acoustic beam in the *yz* plane at $x = 0$ mm. (c) Simulated acoustic beam in the *xy* plane at $z = 20$ mm. (d) Hydrophone-measured 3-D acoustic field. (e) Measured acoustic beam in the *yz* plane at $x = 0$ mm. (f) Measured acoustic beam in the *xy* plane at $z = 20$ mm. A dynamic range of 15 dB was used.

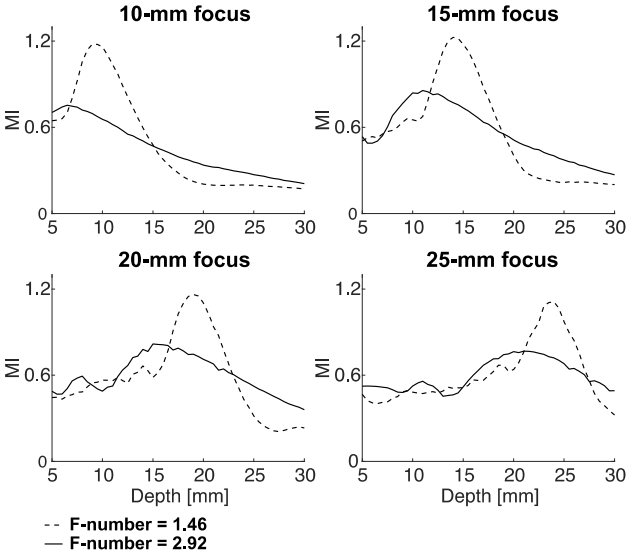

Fig. 4. MI measurements of the push beams with different focal depths (10–25 mm) and different *F*-numbers (1.46 and 2.92).

at 15 mm depth with an *F*-number of 1.46, and the maximum $I_{\mathrm{SPTA},0.3}$ measured was 132.09 mW/cm^2 with a 1 Hz PRF, which are both well below the Food and Drug Administration (FDA) regulatory limit [42].

B. Elasticity Phantom Studies

Fig. 5(a) presents the representative 3-D shear wave motions induced by the comb-push beams using the RCA array in the homogenous phantom. Shear waves were successfully induced by ARF and propagated across the full FOV in two opposite directions (positive *y*-direction and negative *y*-direction). Fig. 5(b) shows the reconstructed 3-D SWS map of the homogenous phantom, as well as the histogram. The measured SWS was 2.63 ± 0.13 m/s, which was well matched with the reference value (2.60 ± 0.15 m/s) from the literature [40]. The results from the in vitro homogenous phantom study demonstrated that the proposed method could successfully perform 3-D shear wave detection with ultrafast volume rate (e.g., 2000 Hz) and reconstruct the full 3-D SWS map with high accuracy.

Fig. 6 demonstrates representative shear wave motions in the region containing a stiff spherical lesion (Type IV, 64.9 kPa) with higher SWS (4.65 m/s) compared to the background (2.45 m/s). As indicated by the arrows in Fig. 6, the shear waves accelerated when propagating through the lesion. The reconstructed 3-D SWS map is shown in Fig. 7, from which one can see the reconstructed SWS image was well aligned with the spherical lesion in the B-mode image [see Fig. 7(a) and (b)], and the lesion was clearly reconstructed in 3-D with a spherical shape [Fig. 7(c)]. The measured volume of the segmented spherical lesion by thresholding (2.95 m/s) was 0.59 mL, which was matched with the nominal volume of the lesion (0.60 mL). Furthermore, the correlation coefficient for SWS estimation over the volume was 0.91 ± 0.04, which indicates a high-quality SWS estimation.

Fig. 8 shows the 3-D SWS results of four different types of lesions. The spherical lesions with different shear wave speed values can be clearly visualized [Fig. 8(a)]. As shown in Fig. 8(b), for lesion type I, the reference SWS was 1.38 m/s and the measured SWS was 1.86 ± 0.05 m/s (10.4 kPa); for lesion type II, the reference SWS was 1.83 m/s and the measured SWS was 2.00 ± 0.03 m/s (12 kPa); for lesion type III, the reference SWS was 3.45 m/s and the measured SWS value was 2.72 ± 0.03 m/s (22.2 kPa); for lesion type IV, the reference SWS was 4.65 m/s and the measured SWS value was 3.37 ± 0.09 m/s (34.1 kPa); and for background, the reference SWS was 2.45 m/s and the measured SWS value was 2.36 ± 0.06 m/s (16.7 kPa). The quantitative measurements show that the proposed method can differentiate different lesions based on measured shear wave speeds. However, the calculated SWS values were overestimated for soft lesions and underestimated for stiff lesions, the biased measurements may be due to the partial volume effect and spatial resolution limit of the proposed method, which resulted from the limited number of compounding angles for high volume rate and RCA layout (i.e., only one-way focusing along the *x*- and *y*-direction).

C. In Vivo Case Study

Fig. 9 shows the in vivo B-mode images and SWS images in the breast of a volunteer using clinical 2-D ultrasound systems and the proposed 3-D ARF-SWE method. The B-mode image from the conventional clinical scanner shows a breast mass, and the corresponding 2-D SWS image indicates a mass with high stiffness [see Fig. 9(a) and (b)]. The RCA array shows similar results with a stiff lesion. The reference SWS measurement using the 2-D SWE from the conventional clinical system was 6.60 m/s (130.7 kPa), and the measured SWS using the proposed method was 8.43 m/s (213.2 kPa). The higher SWS value from RCA may be a result of probe compression during scanning, which was necessary because of the suboptimal B-mode imaging quality of the RCA. The measured volume of the stiff lesion segmented

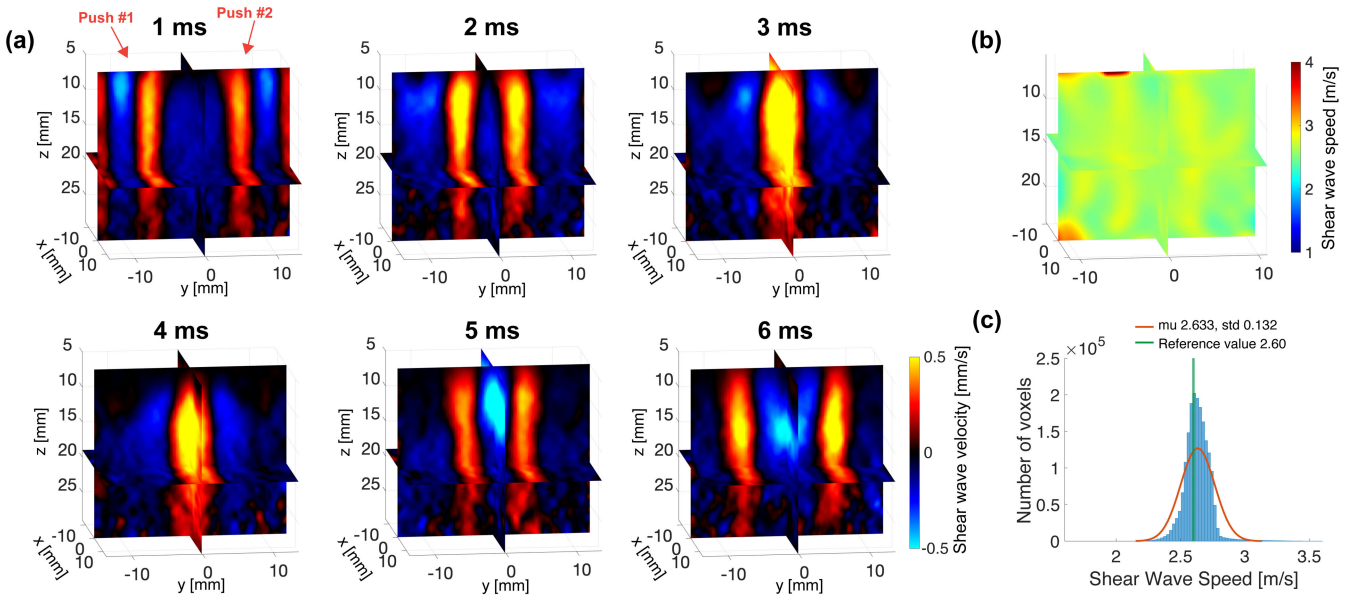

Fig. 5. Three-dimensional shear wave motions and reconstructed 3-D SWS map of the homogenous phantom using the proposed 3-D SWE method. (a) Tri-plane view of the 3-D shear wave motions induced by comb-push beams at different representative time points, and the detection volume rate was 2000 Hz. (b) Tri-plane view of the reconstructed 3-D SWS map. (c) SWS histogram of the full volume.

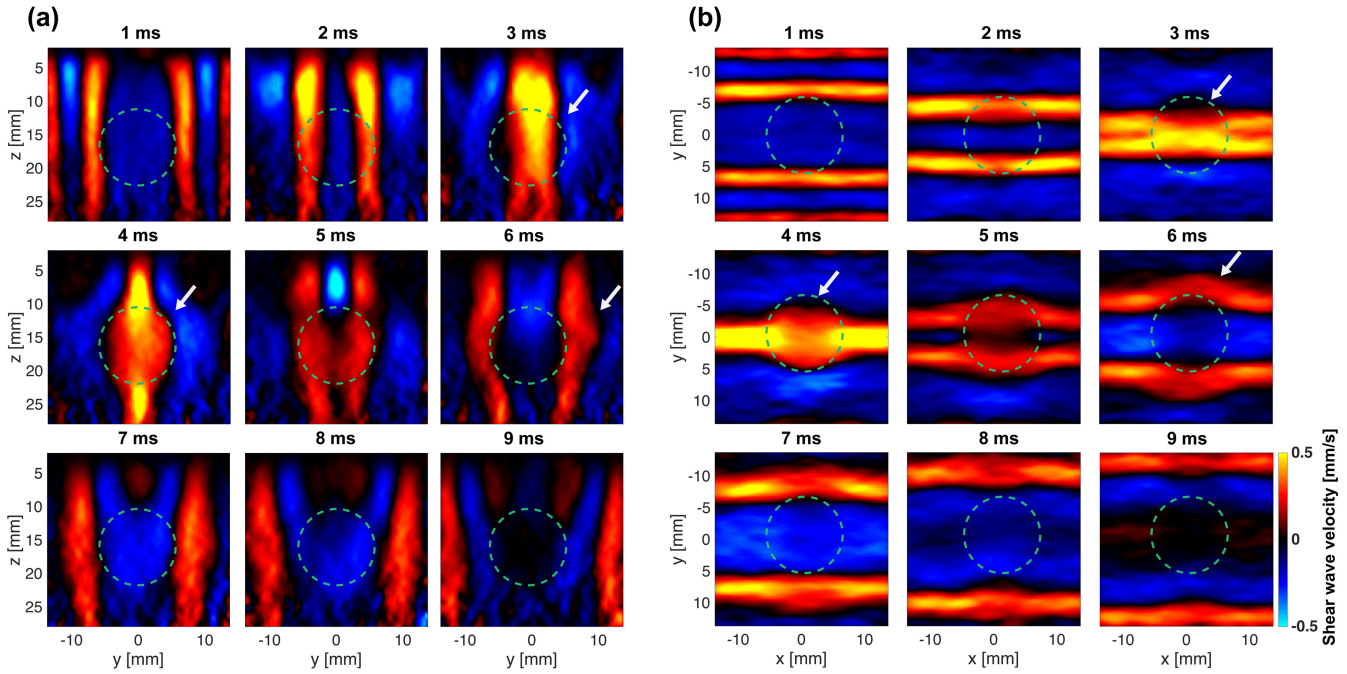

Fig. 6. Shear wave motions at representative time points along (a) *yz* plane and (b) *xy* plane in the elasticity phantom including a stiff spherical lesion object. The contour of the spherical lesion is indicated using the green dashed circle.

using thresholding (3 m/s) was 6.71 mL, and the calculated correlation coefficient over the volume was 0.56 ± 0.12.

IV. Discussion

Previously we developed an RCA-based 3-D shear wave motion detection technique that utilized external vibration to perform 3-D SWE [32]. RCA arrays provide an ultrafast volume rate (e.g., 2000 Hz) with a short acquisition time (e.g., tens of milliseconds), which is ideal for practical implementations of the 3-D SWE technology. In this study, we further developed the 3-D SWE technique to perform ARF-based SWE using the same RCA probe. We incorporated the CUSE technique in our study to achieve fast and full FOV 3-D SWS reconstruction. In this study, we demonstrated that the proposed method could reconstruct a 3-D SWE map using a single push-detect data acquisition (15.4 ms) at an ultrafast volume rate (e.g., 2000 Hz). The acoustic field scanning illustrated that the RCA array could generate robust push beams with adequate ARF. The RCA was able to withstand the long-duration push pulses without causing any damage to the probe. The quantitative and qualitative results from

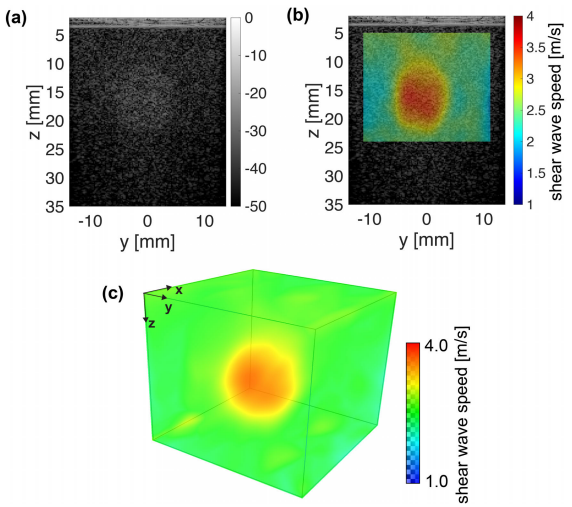

Fig. 7. Reconstructed 3-D SWS map of the elasticity phantom, including a stiff spherical lesion object. (a) *yz* slice of the B-mode image by the RCA array, (b) *yz* slice of the SWS map overlapped on the B-mode image, and (c) volumetric view.

elasticity phantom studies and an in vivo study demonstrated that the 3-D shear wave motions and 3-D elasticity map could be successfully detected and reconstructed by the proposed method, respectively. Furthermore, the in vivo breast imaging results showcase the human imaging capacity of our method, indicating a clear path toward clinical implementation.

Compared to the external vibration-based 3-D SWE, the ARF-based 3-D SWE method is more efficient and convenient because there is no need for additional equipment (e.g., vibrators and related electronic equipment), and push and detection can be performed using only the RCA array. Furthermore, compared to the low frequencies used by the external vibration (e.g., harmonic within the range of 50–200 Hz), the shear waves induced by the ARF have a broader spectrum (e.g., 75–500 Hz [43]), corresponding to smaller shear wave wavelength and better spatial resolution for the reconstructed SWS map.

One significant advantage of the proposed method compared to the clinical 3-D SWE technologies is that the proposed method could perform true 3-D shear wave detection with sufficient ARF at an ultrafast volume rate (e.g., thousands of Hertz). The conventional 3-D SWE technique is based on the mechanical translation of the 1-D array (e.g., wobblers), which limits the shear wave detection in 2-D planes, and the inter plane shear wave motions cannot be retrieved. For 3-D SWE methods based on 2-D matrix arrays using ARF, the FOV is largely limited (e.g., $19.2 \times 19.2 \times 20$ mm^3 for a 32×32 array with 1024 channels [25]), and increasing the number of channels (e.g., several thousand) for enlarged FOV is technically challenging, which also restricts their clinical feasibility. Furthermore, as the multiplexer is necessary to reduce the number of physical channels in 2-D matrix arrays, the volume rate is significantly reduced (e.g., hundreds of Hertz), and the delicate circuitry related to the multiplexers is susceptible to damage caused by the long-duration push pulses. Thanks to the unique design of the RCA array, the proposed method with shear wave generation and 3-D detection capabilities is compatible with clinical ultrasound systems and has a clear pathway for future clinical translation.

Another benefit of the proposed method is that the whole 3-D elasticity map reconstruction can be done using a single push event with the comb-push beams. One issue related to the ARF-based SWE is that the shear wave speed cannot be retrieved in the focused beam region. By simultaneously transmitting two push beams from both sides of the RCA array, the focal region of the push beam is covered by the shear waves induced by the other push beam from the opposite side, as shown in Fig. 2. The proposed method used comb-push beams (0.4 ms) and continuous acquisition of 30 volumes (15 ms) at 2000 Hz, leading to a total acquisition time of 15.4 ms, which was fast enough to avoid tissue motions and handheld probe movement. Moreover, the patient did not need to hold their breath for several seconds during the data acquisition, which was a common practice for conventional 3-D SWE techniques. Note that the number of acquired volumes needs to be increased for low shear wave speed estimation (e.g., 1 m/s), otherwise, the reconstruction FOV will be limited.

Besides the spherical elasticity objects evaluated in Section III-B, the proposed method also has the capability of detecting small stiffness objects from the background. A cylindrical elasticity target, located at around 33 mm depth, with a diameter of 4.05 mm and SWS of 4.84 m/s (70.2 kPa, Model 049A, CIRS Inc., Norfolk, VA, USA) was imaged using the proposed 3-D ARF-SWE method. As shown in Fig. 10, the cylindrical elasticity target can be clearly distinguished from the background (16.4 kPa, SWS of 2.34 m/s).

One limitation of the proposed method is related to the spatial resolution of RCA arrays, which is suboptimal because of the one-way focusing (e.g., either transmit or receive focusing along x- or y-direction, no two-way focusing in both dimensions). As an example, when transmitting using row elements (distributed along the x-direction) and receiving using column elements (distributed along the y-direction), as indicated in Fig. 1, the transmit focusing is along the x-direction, and the receive focusing is along the y-direction, which is different from two-way focusing of the 2-D matrix array. To achieve ultrafast volume rate (i.e., thousands of Hertz) as required for ARF-induced shear wave detection without aliasing, the number of compounding angles is limited (e.g., seven angles used in this study), resulting in suboptimal spatial resolution along x-direction as shown in Fig. 1(b), where only transmit focusing was available, and therefore the spatial resolution is strictly dictated by the number and range of compounding angles [44]. Therefore, the spatial resolution along the transmit focusing of the reconstructed SWS map was worse than the one in the other direction, as shown in Fig. 8. This limitation can be alleviated by applying more compounding angles, implementing the row transmit and column receive (RC) + column transmit and row receive (CR) scheme [45], or using other transmit schemes such as synthetic aperture imaging [46]; however, the volume rate will be reduced, and multiple push-detection data acquisition cycles may be needed to synthesize a high volume rate acquisition.

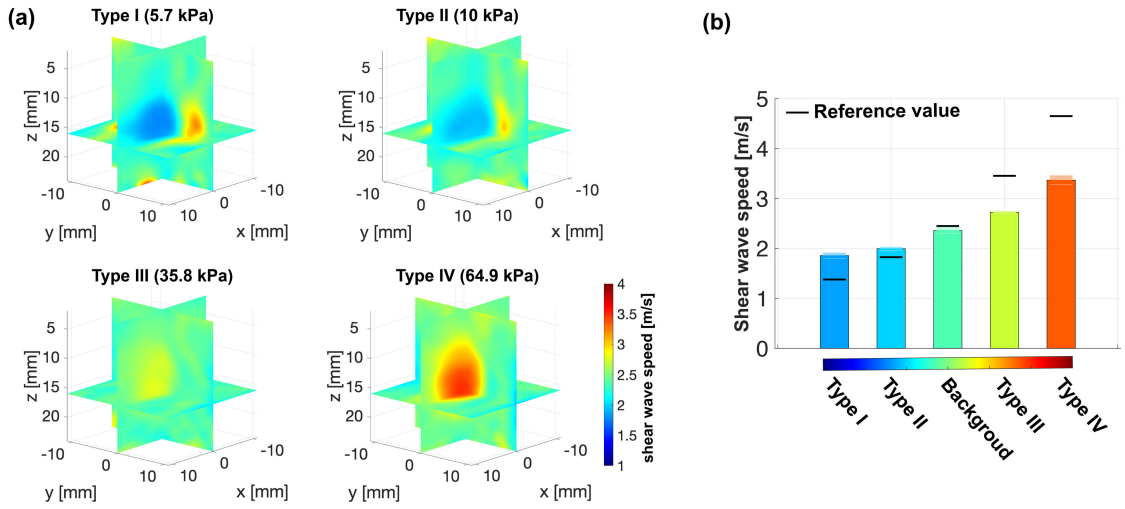

Fig. 8. Reconstructed SWS maps and calculated SWS values of four different types of spherical lesions. (a) Tri-plane view of reconstructed SWS maps. Corresponding Young's modulus is labeled. (b) Calculated SWS values of four types of lesion objects and the background of the elasticity phantom. The corresponding standard deviation and reference values (black line) are labeled.

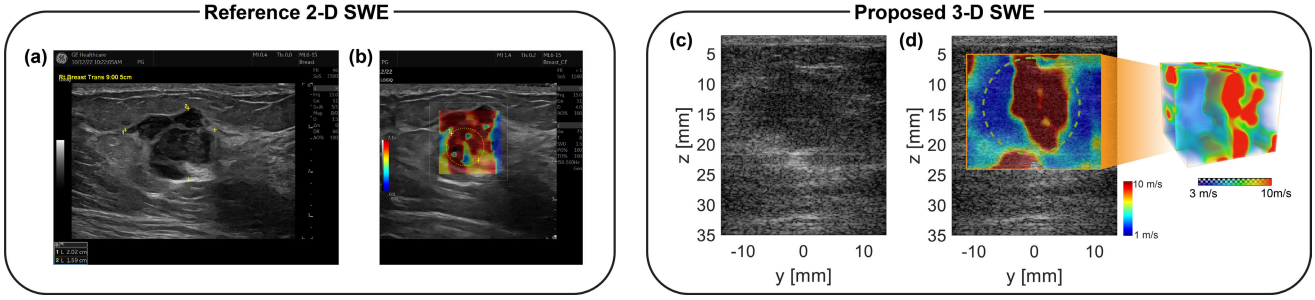

Fig. 9. B-mode and SWE imaging of a breast lesion with the reference 2-D SWE method and the proposed 3-D ARF-SWE method. (a) Conventional B-mode image of a breast mass using the clinical scanner. (b) Two-dimensional SWE using the clinical scanner. (c) B-mode image along the *yz* slice using the RCA array. (d) Reconstructed 3-D SWS map and the *yz* slice using the proposed 3-D SWE method. The SWS measurement ROIs are labeled in (b) and (d).

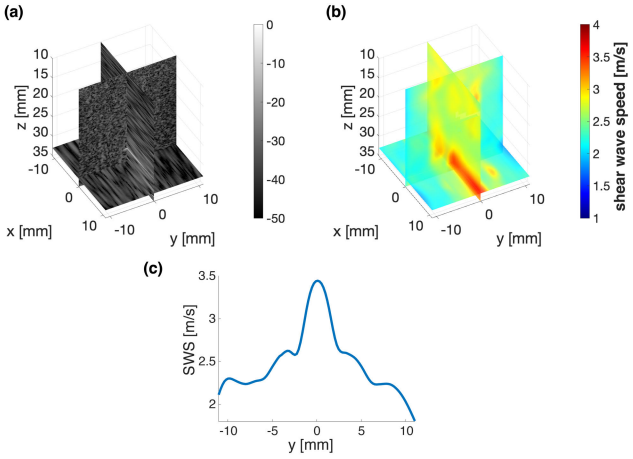

Fig. 10. Reconstructed 3-D SWS map of the elasticity phantom, including a stiff cylindrical lesion object. (a) Tri-plane view B-mode imaging for the phantom. (b) Tri-plane view of the reconstructed SWS map of the lesion object. (c) SWS profile along the *y*-direction at the *x* location of 0 mm and depth of 33 mm.

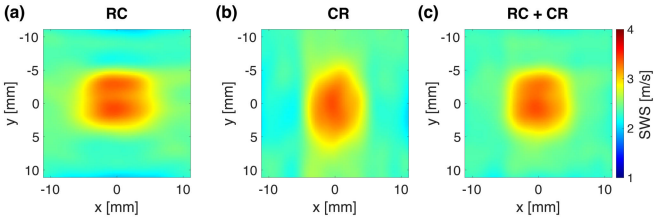

Fig. 11. Reconstructed SWS map of the Type IV spherical inclusion in the *xy* plane at 15-mm depth using (a) column push, and detection with RC, (b) row push, and detection with CR, and (c) combination of RC and CR using averaging.

As demonstrated in Fig. 11, the SWS map can be reconstructed using column element to push, and detection with RC scheme [see Fig. 11(a)], or using row element to push, and detection with CR scheme [see Fig. 11(b)]. A symmetrical inclusion can be reconstructed by combining the RC and CR [see Fig. 11(c)] using two sequential push-detection acquisitions.

Another limitation of the proposed RCA-based 3-D ARF-SWE method is that unlike 2-D matrix arrays that can generate cylindrically shaped push beams with omnidirectional shear waves that are capable of providing tissue anisotropy estimation [25], RCA-array-induced shear waves are planar and therefore limited to only providing sensitivity to tissue anisotropy along the wave propagation direction (e.g., either *x*- or *y*-direction). One potential solution to overcome

this constraint is the adoption of a novel RCA design featuring bias-switchable capabilities [47]. This advanced design could potentially generate cylindrically shaped push beams to provide shear waves that propagate both along the x- and y-direction.

Compared to other 3-D ultrasound elastography methods utilizing matrix arrays [48], RCA arrays do not use multiplexing, thereby enabling ARF-based SWE. In general, ARF-based SWE techniques are more convenient in practice because of the absence of external shear wave sources (e.g., electromechanical shakers). In addition, ARF-SWE techniques do not involve complex boundary conditions or wave interferences that are typical with continuous shear waves that are mechanically produced. In addition, the low element count of RCA arrays also makes ultrafast 3-D imaging easily attainable (e.g., 2000 Hz volume rate), which is essential for robust shear wave detection. The low channel count also makes RCA arrays compatible with mainstream ultrasound systems, providing a clear pathway for future clinical translations and wide dissemination of the 3-D SWE technologies developed based on this probe. The major disadvantage of RCA arrays is the suboptimal imaging quality when compared to matrix arrays, which leads to spatially broadened shear wave signals that result in blurred SWS maps with estimation bias. Nevertheless, based on the promising 3-D SWE results presented in this article, a future study dedicated to improving the B-mode imaging quality of RCA arrays in the context of 3-D shear wave detection is warranted.

To enhance the imaging quality of the reference B-mode imaging for overlapping between the B-mode image and elasticity image, a high-quality B-mode image can be immediately acquired before or after the shear wave acquisition using a large number of compounding angles or other transmission schemes such as synthetic aperture transmission or wide beams [32].

The imaging quality of 3-D elasticity maps depends on two major factors: shear wave signal quality (e.g., shear wave SNR and spectrum, which is largely dictated by the power of the push beam) and shear wave detection imaging quality (e.g., ultrasound imaging SNR and spatial resolution). As discussed, the detection imaging quality is related to the intrinsic limitations associated with the RCA probe design. The phantom studies showed that the SWS measurements of the lesion objects were biased when compared to the reference SWS values, which could result from the partial volume effect and suboptimal spatial resolution related to the RCA array. Ongoing studies are being conducted to further optimize the sequence and processing to address the biasing issue.

Although the current RCA array provides sufficient ARF for inducing shear waves, its MI is lower than conventional 1-D probes (e.g., MI of 1.5 or higher [32]). As a result, the generated shear waves are weaker than conventional 1-D ultrasound, posing a challenge for clinical studies. To achieve higher MI values for strong shear wave signals, the F-number can be reduced with more activated elements at each transmission. Furthermore, multiple push events can be used to improve SNR and contrast, for example, comb-push beams could be applied multiple times with different push locations, and then compound to the final elastography image. Meanwhile, a better RCA probe design and manufacturing is necessary to improve the quality of the probes, and further work can be conducted to optimize the probe performance for better shear wave generation.

V. Conclusion

In this study, we presented a novel 3-D SWE method using a 2-D row-column-addressing (RCA) array for both shear wave generation (i.e., using ARF) and detection. The proposed 3-D SWE method provides 3-D shear wave speed maps with an ultrafast shear wave motion detection volume rate (e.g., 2000 Hz). We integrated the CUSE technique into our approach, resulting in a fast 3-D SWE sequence with a total data acquisition time of approximately 16 ms. In vitro and in vivo results demonstrated the robust performance of the proposed 3-D SWE technique, which provides a practical and cost-effective 3-D SWE solution for clinical implementations of 3-D tissue elasticity imaging.

Acknowledgment

Opinions, interpretations, conclusions, and recommendations are those of the author and are not necessarily endorsed by the Department of Defense.

Zhijie Dong and Matthew R. Lowerison are with the Department of Electrical and Computer Engineering, Beckman Institute for Advanced Science and Technology, University of Illinois Urbana-Champaign, Urbana, IL 61801 USA (e-mail: zhijied3@illinois.edu; mloweri@illinois.edu).

U-Wai Lok, Chengwu Huang, and Shigao Chen are with the Department of Radiology, Mayo Clinic College of Medicine and Science, Rochester, MN 55905 USA (e-mail: lok.u-wai@mayo.edu; huang.chengwu@mayo.edu; chen.shigao@mayo.edu).

Pengfei Song is with the Department of Electrical and Computer Engineering, the Department of Bioengineering, the Beckman Institute for Advanced Science and Technology, The Carle Illinois College of Medicine, the Cancer Center at Illinois, and the Neuroscience Program, University of Illinois Urbana-Champaign, Urbana, IL 61801 USA (e-mail: songp@illinois.edu).

References

[1] F. Sebag et al., "Shear wave elastography: A new ultrasound imaging mode for the differential diagnosis of benign and malignant thyroid nodules," *J. Clin. Endocrinol. Metabolism*, vol. 95, no. 12, pp. 5281–5288, 2010.

[2] P. Lin, M. Chen, B. Liu, S. Wang, and X. Li, "Diagnostic performance of shear wave elastography in the identification of malignant thyroid nodules: A meta-analysis," *Eur. Radiol.*, vol. 24, pp. 2729–2738, 2014.

[3] G. Ferraioli, P. Parekh, A. B. Levitov, and C. Filice, "Shear wave elastography for evaluation of liver fibrosis," *J. Ultrasound Med.*, vol. 33, no. 2, pp. 197–203, Feb. 2014.

[4] G. Ferraioli et al., "Accuracy of real-time shear wave elastography for assessing liver fibrosis in chronic hepatitis C: A pilot study," *Hepatology*, vol. 56, no. 6, pp. 2125–2133, 2012.

[5] A. Evans et al., "Invasive breast cancer: Relationship between shear-wave elastographic findings and histologic prognostic factors," *Radiology*, vol. 263, no. 3, pp. 673–677, 2012.

[6] J. Ophir, "Elastography: A quantitative method for imaging the elasticity of biological tissues," *Ultrason. Imag.*, vol. 13, no. 2, pp. 111–134, Apr. 1991.

[7] J.-L. Gennisson, T. Deffieux, M. Fink, and M. Tanter, "Ultrasound elastography: Principles and techniques," *Diagnostic Intervent. Imag.*, vol. 94, no. 5, pp. 487–495, May 2013.

[8] K. Nightingale, "Acoustic radiation force impulse (ARFI) imaging: A review," *Current Med. Imag. Rev.*, vol. 7, no. 4, pp. 328–339, Nov. 2011.

[9] R. M. Sigrist, J. Liau, A. El Kaffas, M. C. Chammas, and J. K. Willmann, "Ultrasound elastography: Review of techniques and clinical applications," *Theranostics*, vol. 7, no. 5, p. 1303, 2017.

[10] T. Shiina et al., "WFUMB guidelines and recommendations for clinical use of ultrasound elastography: Part 1: Basic principles and terminology," *Ultrasound Med. Biol.*, vol. 41, no. 5, pp. 1126–1147, May 2015.

[11] R. G. Barr et al., "WFUMB guidelines and recommendations for clinical use of ultrasound elastography: Part 2: Breast," *Ultrasound Med. Biol.*, vol. 41, no. 5, pp. 1148–1160, May 2015.

[12] L. Sandrin et al., "Transient elastography: A new noninvasive method for assessment of hepatic fibrosis," *Ultrasound Med. Biol.*, vol. 29, no. 12, pp. 1705–1713, Dec. 2003.

[13] L. Huwart et al., "Liver fibrosis: Non-invasive assessment with MR elastography," *NMR Biomed., Int. J. Devoted Develop. Appl. Magn. Reson. vivo*, vol. 19, no. 2, pp. 173–179, 2006.

[14] A. P. Sarvazyan, O. V. Rudenko, S. D. Swanson, J. B. Fowlkes, and S. Y. Emelianov, "Shear wave elasticity imaging: A new ultrasonic technology of medical diagnostics," *Ultrasound Med. Biol.*, vol. 24, no. 9, pp. 1419–1435, Dec. 1998.

[15] J. Bercoff, M. Tanter, and M. Fink, "Supersonic shear imaging: A new technique for soft tissue elasticity mapping," *IEEE Trans. Ultrason., Ferroelectr., Freq. Control*, vol. 51, no. 4, pp. 396–409, Apr. 2004.

[16] C. Papadacci, V. Finel, O. Villemain, M. Tanter, and M. Pernot, "4D ultrafast ultrasound imaging of naturally occurring shear waves in the human heart," *IEEE Trans. Med. Imag.*, vol. 39, no. 12, pp. 4436–4444, Dec. 2020.

[17] P. Santos et al., "Natural shear wave imaging in the human heart: Normal values, feasibility, and reproducibility," *IEEE Trans. Ultrason., Ferroelectr., Freq. Control*, vol. 66, no. 3, pp. 442–452, Mar. 2019.

[18] M. Wang, B. Byram, M. Palmeri, N. Rouze, and K. Nightingale, "Imaging transverse isotropic properties of muscle by monitoring acoustic radiation force induced shear waves using a 2-D matrix ultrasound array," *IEEE Trans. Med. Imag.*, vol. 32, no. 9, pp. 1671–1684, Sep. 2013.

[19] P. Song et al., "Quantitative assessment of left ventricular diastolic stiffness using cardiac shear wave elastography: A pilot study," *J. Ultrasound Med.*, vol. 35, no. 7, pp. 1419–1427, Jul. 2016.

[20] W.-N. Lee et al., "Mapping myocardial fiber orientation using echocardiography-based shear wave imaging," *IEEE Trans. Med. Imag.*, vol. 31, no. 3, pp. 554–562, Mar. 2012.

[21] D. C. Mellema et al., "Probe oscillation shear wave elastography: Initial in vivo results in liver," *IEEE Trans. Med. Imag.*, vol. 37, no. 5, pp. 1214–1223, May 2018.

[22] S. K. Venkatesh, M. Yin, and R. L. Ehman, "Magnetic resonance elastography of liver: Technique, analysis, and clinical applications," *J. Magn. Reson. Imag.*, vol. 37, no. 3, pp. 544–555, 2013.

[23] J. Tian, Q. Liu, X. Wang, P. Xing, Z. Yang, and C. Wu, "Application of 3D and 2D quantitative shear wave elastography (SWE) to differentiate between benign and malignant breast masses," *Sci. Rep.*, vol. 7, no. 1, pp. 1–9, 2017.

[24] C. K. Zhao et al., "Three-dimensional shear wave elastography for differentiating benign from malignant thyroid nodules," *J. Ultrasound Med.*, vol. 37, no. 7, pp. 1777–1788, 2018.

[25] J. Gennisson et al., "4-D ultrafast shear-wave imaging," *IEEE Trans. Ultrason., Ferroelectr., Freq. Control*, vol. 62, no. 6, pp. 1059–1065, Jun. 2015.

[26] C. Huang et al., "Three-dimensional shear wave elastography on conventional ultrasound scanners with external vibration," *Phys. Med. Biol.*, vol. 65, no. 21, Nov. 2020, Art. no. 215009.

[27] J. T. Yen and S. W. Smith, "Real-time rectilinear 3-D ultrasound using receive mode multiplexing," *IEEE Trans. Ultrason., Ferroelectr., Freq. Control*, vol. 51, no. 2, pp. 216–226, Feb. 2004.

[28] C. Risser, H. J. Welsch, H. Fonfara, H. Hewener, and S. Tretbar, "High channel count ultrasound beamformer system with external multiplexer support for ultrafast 3D/4D ultrasound," in *Proc. IEEE Int. Ultrason. Symp. (IUS)*, Sep. 2016, pp. 1–4.

[29] S. Blaak et al., "Design of a micro-beamformer for a 2D piezoelectric ultrasound transducer," in *Proc. IEEE Int. Ultrason. Symp.*, Sep. 2009, pp. 1338–1341.

[30] G. Matrone, A. S. Savoia, M. Terenzi, G. Caliano, F. Quaglia, and G. Magenes, "A volumetric CMUT-based ultrasound imaging system simulator with integrated reception and μ-beamforming electronics models," *IEEE Trans. Ultrason., Ferroelectr., Freq. Control*, vol. 61, no. 5, pp. 792–804, May 2014.

[31] C. E. Morton and G. R. Lockwood, "Theoretical assessment of a crossed electrode 2-D array for 3-D imaging," in *Proc. IEEE Symp. Ultrasonics*, vol. 1, Oct. 2003, pp. 968–971.

[32] Z. Dong et al., "Three-dimensional shear wave elastography using a 2D row column addressing (RCA) array," *BME Frontiers*, vol. 2022, Mar. 2022, Art. no. 9879632, doi: 10.34133/2022/9879632.

[33] M. Bernal, N. Benech, R. Daigle, and J. Brum, "Towards 3D passive shear elasticity imaging using row-columns arrays," in *Proc. IEEE Int. Ultrason. Symp. (IUS)*, Sep. 2021, pp. 1–4.

[34] P. Song et al., "Two-dimensional shear-wave elastography on conventional ultrasound scanners with time-aligned sequential tracking (TAST) and comb-push ultrasound shear elastography (CUSE)," *IEEE Trans. Ultrason., Ferroelectr., Freq. Control*, vol. 62, no. 2, pp. 290–302, Feb. 2015.

[35] P. Song, M. W. Urban, A. Manduca, H. Zhao, J. F. Greenleaf, and S. Chen, "Comb-push ultrasound shear elastography (CUSE) with various ultrasound push beams," *IEEE Trans. Med. Imag.*, vol. 32, no. 8, pp. 1435–1447, Aug. 2013.

[36] J. Sauvage et al., "4D functional imaging of the rat brain using a large aperture row-column array," *IEEE Trans. Med. Imag.*, vol. 39, no. 6, pp. 1884–1893, Jun. 2020.

[37] G. F. Pinton, J. J. Dahl, and G. E. Trahey, "Rapid tracking of small displacements with ultrasound," *IEEE Trans. Ultrason., Ferroelectr., Freq. Control*, vol. 53, no. 6, pp. 1103–1117, Jun. 2006.

[38] C. Kasai, K. Namekawa, A. Koyano, and R. Omoto, "Real-time two-dimensional blood flow imaging using an autocorrelation technique," *IEEE Trans. Sonics Ultrason.*, vol. SU-32, no. 3, pp. 458–464, May 1985.

[39] P. Song, A. Manduca, H. Zhao, M. W. Urban, J. F. Greenleaf, and S. Chen, "Fast shear compounding using robust 2-D shear wave speed calculation and multi-directional filtering," *Ultrasound Med. Biol.*, vol. 40, no. 6, pp. 1343–1355, Jun. 2014.

[40] H. Zhao et al., "External vibration multi-directional ultrasound shearwave elastography (EVMUSE): Application in liver fibrosis staging," *IEEE Trans. Med. Imag.*, vol. 33, no. 11, pp. 2140–2148, Nov. 2014.

[41] S. Cournane, A. Fagan, and J. Browne, "Review of ultrasound elastography quality control and training test phantoms," *Ultrasound*, vol. 20, no. 1, pp. 16–23, 2012.

[42] B. A. Herman and G. R. Harris, "Models and regulatory considerations for transient temperature rise during diagnostic ultrasound pulses," *Ultrasound Med. Biol.*, vol. 28, no. 9, pp. 1217–1224, Sep. 2002.

[43] M. L. Palmeri and K. R. Nightingale, "Acoustic radiation force-based elasticity imaging methods," *Interface Focus*, vol. 1, no. 4, pp. 553–564, 2011.

[44] G. Montaldo, M. Tanter, J. Bercoff, N. Benech, and M. Fink, "Coherent plane-wave compounding for very high frame rate ultrasonography and transient elastography," *IEEE Trans. Ultrason., Ferroelectr., Freq. Control*, vol. 56, no. 3, pp. 489–506, Mar. 2009.

[45] M. Flesch et al., "4D in vivo ultrafast ultrasound imaging using a row-column addressed matrix and coherently-compounded orthogonal plane waves," *Phys. Med. Biol.*, vol. 62, no. 11, p. 4571, 2017.

[46] H. Bouzari, M. Engholm, S. I. Nikolov, M. B. Stuart, E. V. Thomsen, and J. A. Jensen, "Imaging performance for two row-column arrays," *IEEE Trans. Ultrason., Ferroelectr., Freq. Control*, vol. 66, no. 7, pp. 1209–1221, Jul. 2019.

[47] M. R. Sobhani, M. Ghavami, A. K. Ilkhechi, J. Brown, and R. Zemp, "Ultrafast orthogonal row–column electronic scanning (uFORCES) with bias-switchable top-orthogonal-to-bottom electrode 2-D arrays," *IEEE Trans. Ultrason., Ferroelectr., Freq. Control*, vol. 69, no. 10, pp. 2823–2836, Oct. 2022.

[48] H. S. Hashemi, S. K. Mohammed, Q. Zeng, R. Z. Azar, R. N. Rohling, and S. E. Salcudean, "3-D ultrafast shear wave absolute vibro-elastography using a matrix array transducer," *IEEE Trans. Ultrason., Ferroelectr., Freq. Control*, vol. 70, no. 9, pp. 1039–1053, Sep. 2023.

Zhijie Dong (Member, IEEE) received the B.Eng. degree in information engineering from Southeast University, Nanjing, China, in 2017, the M.S. degree in electrical and computer engineering from the University of Michigan, Ann Arbor, MI, USA, in 2018, and the Ph.D. degree in electrical and computer engineering from the University of Illinois Urbana-Champaign, Urbana, IL, USA, in 2023.

His research interests are ultrafast 3-D ultrasound imaging and deep learning in ultrasound.

U-Wai Lok received the Ph.D. degree from the Institute of Biomedical Electronics and Bioinformatics, Department of Electrical Engineering, National Taiwan University, Taipei, Taiwan, in 2017.

He was a Member of the Electrical Engineer with Sunplus Technology, Hsinchu, Taiwan, where his work was focused on wireless communication protocol, embedded system design, and signal processing. He is currently with the Department of Radiology, Mayo Clinic College of Medicine, Rochester, MN, USA. His current research interests include ultrasonic microvessel imaging, deep learning, super resolution ultrasound microvessel imaging, ultrasound localization microscopy, and 3-D ultrasound imaging.

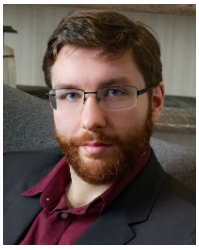

Matthew R. Lowerison received the Ph.D. degree in medical biophysics from the University of Western Ontario, London, ON, Canada, in 2017.

He is now with the Department of Electrical and Computer Engineering and the Beckman Institute for Advanced Science and Technology, University of Illinois at Urbana-Champaign, Urbana, IL, USA. His current research interests include ultrasound microvessel imaging, super resolution ultrasound localization microscopy, and ultrasonic characterization of neurological disorders and tumor microenvironments.

Chengwu Huang (Member, IEEE) received the Ph.D. degree from the Department of Biomedical Engineering, Tsinghua University, Beijing, China, in 2017.

He is currently an Assistant Professor with the Department of Radiology, Mayo Clinic College of Medicine, Rochester, MN, USA. His current research interests include ultrasound microvessel imaging, ultrasound beamforming, and ultrasound elastography.

Shigao Chen (Senior Member, IEEE) received the Ph.D. degree in biomedical imaging from the Mayo Graduate School, Rochester, MN, in 2002.

He is currently a Professor of the Mayo Clinic College of Medicine, Rochester, MN, USA. His current research interests include ultrasound beamforming, shear wave elastography, liver steatosis quantification, and microvessel imaging.

Pengfei Song (Senior Member, IEEE) received the Ph.D. degree in biomedical engineering from Mayo Clinic College of Medicine, Rochester, MN, USA, in 2014, under the supervision of Dr. James Greenleaf and Dr. Shigao Chen.

He is currently a Y. T. Lo Faculty Fellow and an Assistant Professor with the Department of Electrical and Computer Engineering and the Beckman Institute, University of Illinois Urbana-Champaign, Urbana, IL, USA. He has authored or coauthored over 90 peer reviewed journal articles in the field of ultrasound imaging. He holds several patents that have been licensed and commercialized by major ultrasound companies and used worldwide in the clinic. His research interests include super resolution ultrasound imaging, ultrafast 3-D imaging, deep learning, functional ultrasound, and ultrasound shear wave elastography.

Dr. Song was a recipient of the NIH K99/R00 Pathway to Independence Award, the NSF CAREER Award, the NIH/NIBIB Trailblazer Award, the IEEE Ultrasonics Early Career Investigator Award, and the Chan Zuckerberg Initiative (CZI) Early Career Acceleration Award. He is a fellow member of the American Institute of Ultrasound in Medicine, a Senior Member of the National Academy of Inventors, and a Full Member of the Acoustical Society of America.